JOURNAL OF AIRCRAFT
Vol. 31, No. 6, November–December 1994

Flow Visualization Studies on Sidewall Effects in Two-Dimensional Transonic Airfoil Testing

Norikazu Sudani,* Mamoru Sato,† Hiroshi Kanda,† and Kenichi Matsuno‡
National Aerospace Laboratory, Chofu, Tokyo 182, Japan

The effects of sidewall boundary layers in two-dimensional transonic airfoil testing were investigated using oil-flow or liquid crystal visualization techniques. Three different chord models were tested in order to clarify the sidewall effects and to seek a suitable aspect ratio of the airfoil. The oil-flow visualization data systematically reveal the surface flow patterns affected by the sidewalls and suggest a minimum aspect ratio for conducting reliable two-dimensional tests. The results of the liquid crystal visualization also show the three dimensionality of the transition behavior and the necessity of the high aspect ratio. In addition, investigations on effects of the sidewall boundary-layer suction and application of a sidewall interference correction produce significant results for improvement of airfoil testing by removal of the sidewall effects.

Nomenclature

AR = aspect ratio
b = airfoil span
c = airfoil chord
C_d = drag coefficient from wake measurement
C_l = lift coefficient
C_p = pressure coefficient
C_p^* = critical pressure coefficient
d_s = spanwise length of attached flow region near the sidewall (see Fig. 5)
M = Mach number
Re = Reynolds number based on airfoil chord
x = streamwise coordinate
y = spanwise coordinate
α = angle of attack

Subscripts
c = corrected value
g = geometric value
u = uncorrected value

Introduction

IN airfoil testing, effects of the sidewall boundary layers have been one of the most important uncertainties, especially at transonic speeds. Sidewall interference is complicated, and therefore its analysis is necessary for reliable tests. In a two-dimensional airfoil test, comparatively large chord length (in other words, low aspect ratio) models are generally employed in order to realize high Reynolds number flow. Measurements of the surface pressure and the total pressure deficit in the wake are performed in the midspan region that is less affected by the sidewalls. It has become clear, however, that the development of the sidewall boundary layers strongly influences the measurements for such a low aspect ratio model. Because interference of the top and bottom walls was regarded as most important, less research was done on the sidewall problem. Recent investigations have shown, however, that sidewall interference is rather large. While the top and bottom wall influence is essentially inviscid, sidewall interference is viscous and three dimensional.

Figure 1 shows a comparison of pressure distribution data between IAR (the Institute for Aerospace Research, Canada)[1] and NAL (the National Aerospace Laboratory, Japan). Although both are corrected for the top and bottom wall effects only, slight differences in shock wave position and suction peak level ahead of the shock can be recognized. This result suggests that between both data there exists a discrepancy in effective Mach number due to sidewall boundary-layer displacement effect in each wind-tunnel test and, therefore, proposes the necessity for analysis of these complicated effects.

Methods to account for sidewall interference were given by Barnwell[2] and Sewall,[3] and a modified form of a correction considering the effect of airfoil aspect ratio was proposed by Murthy.[4] These theoretical studies are, however, based on various assumptions because of the interference complexity. In experimental studies, on the other hand, global effects of the sidewall have only been discussed and there have been few results of detailed analysis. Su[5] presented the sidewall effects at a relatively low Reynolds number with oil-flow vis-

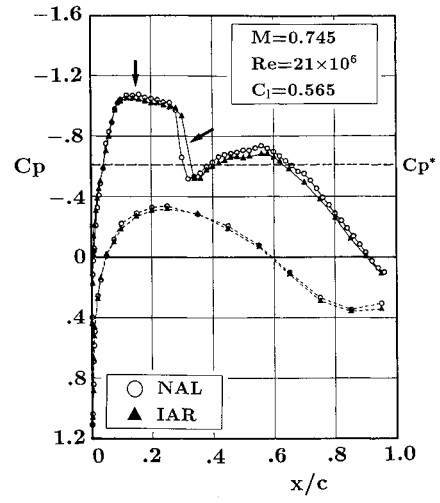

Fig. 1 Comparison of pressure distributions with the same lift coefficient at a corrected Mach number for the top and bottom wall effects of only 0.745.

Received Nov. 3, 1992; presented as Paper 93-0090 at the AIAA 31st Aerospace Sciences Meeting, Reno, NV, Jan. 11–14, 1993; accepted for publication Feb. 24, 1994.

*Research Scientist, Aircraft Aerodynamics Division. Member AIAA.
†Research Scientist, Aircraft Aerodynamics Division.
‡Head of Two-Dimensional Transonic Wind Tunnel Laboratory, Aircraft Aerodynamics Division; currently Associate Professor, Faculty of Engineering, Kyoto Institute of Technology, Kyoto 606, Japan. Member AIAA.

ualization using a high aspect ratio model. In conventional two-dimensional airfoil testing, however, a model with a small chord length cannot realize high Reynolds number tests. Furthermore, although most wind tunnels have a sidewall boundary-layer removal system in the vicinity of the airfoil, few significant results with flow visualization have been shown. It is therefore necessary to analyze the influence of the sidewall systematically for relatively low aspect ratio model with and without the sidewall boundary-layer suction.

In this article, the upper surface flow on a transonic airfoil in a closed test section is systematically analyzed using three different chord models with oil-flow and liquid crystal visualization. The two dimensionality of the surface flow pattern including the transition behavior is discussed, and a suitable model aspect ratio for airfoil testing is evaluated. In addition, the effectiveness of the sidewall boundary-layer suction and the applicability of a sidewall interference correction for removal of the sidewall effects are assessed. It is believed that these visualization studies can provide necessary information for the improvement of airfoil testing. Since interference between the sidewall and the airfoil is very similar to that of the wing-body junction, the studies will also be valuable not only in airfoil testing but also in the clarification of complicated interference of various parts of the aircraft.

Apparatus and Techniques

Wind Tunnel

The tests were conducted in the NAL Two-Dimensional Transonic Wind Tunnel.[6] The wind tunnel is of the blowdown type. Reynolds number based on the airfoil chord length (usually 250 mm) can be varied from 5.5×10^6 to 40×10^6 according to the variation of the stagnation pressure. Mach number can be varied from about 0.2 to 1.15.

The test section of the NAL wind tunnel is 1 m in height, and 0.3 m in width, and is enclosed in a cylindrical plenum chamber. The facility is equipped with a pressure scanning system, a wake traverse system, a schlieren photograph system, and a surface flow visualization system for use with the oil-flow method or the liquid crystal method. The top and bottom walls each have four full slots and two half-slots at the sides and a divergence angle of 0.35 deg for reducing the effect of sidewall boundary-layer development in the empty test section. The open area ratio is normally fixed at 3%, based on the initial calibration tests. Pressure rails are provided on the top and bottom walls for wall interference correction. The sidewalls are, on the other hand, usually solid for the reason mentioned later.

Models

A BGK No. 1 airfoil was selected for these studies because the aerodynamic data measured in the IAR wind tunnel over a wide range of Mach numbers, Reynolds numbers, and angles of attack have already been presented.[1] The data are sufficient for assessment of a sidewall interference correction, and moreover, can be utilized to detect differences in measured data between both wind tunnels and to examine the causes. The BGK No. 1 airfoil is of the supercritical type and designed for shockless flow at a Mach number of 0.75 and a lift coefficient of 0.63.[7] Actually, the shockless flow could be observed at an uncorrected Mach number of 0.772 in the NAL tunnel.

Three models with different chord lengths of 250 mm ($AR = 1.2$), 200 mm ($AR = 1.5$), and 120 mm ($AR = 2.5$) were employed for the oil-flow visualization. They all had a span of 300 mm (the width of the tunnel). The models with chords of 250 and 200 mm were constructed of stainless steel, whereas the model with a chord of 120 mm was made of nickel-chromium-molybdenum steel to make it strong enough for high Reynolds number testing. The models with chords of 200 and 120 mm were dyed black for flow visualization and had no pressure orifice on the surface, whereas the model with a 250-mm chord was made for pressure measurement, and thus the pressure orifices were covered with very thin tape and the surface was painted flat black in these studies.

The models with chords of 250 and 120 mm were employed for liquid crystal visualization. The 250-mm-chord model was made especially for the liquid crystal visualization study. This model was constructed of stainless steel covered with thin ceramics containing zirconia in consideration of progress toward the quantitative measurements. Although the ceramics has a thickness of about 0.5 mm, it is believed to be sufficient for avoiding heat transfer inside the model near the surface. The 120-mm-chord model was the same as the one employed for the oil-flow visualization. Four models in all were used in the visualization studies.

No attempt was made to fix the transition on the models in any of the cases.

Oil-Flow Visualization Technique

Two kinds of oils were used for the flow visualization in these studies. With no sidewall boundary-layer suction, the oil consisted of liquid paraffin, titanium dioxide as a dye, and a little oleic acid. Oil that contains the white powder has the advantage of allowing detailed observations on the model surface flow. With the suction, however, oil containing powder cannot be used because it would damage the sidewall Rigimeshes. For this reason, the combination of a gear oil with a red paint (containing no powder) and the white painted surface can visualize the flow patterns clearly. The visualization data were observed with a charged coupled device (CCD) color video camera mounted outside the test section on the top wall in the plenum chamber and located about 300 mm downstream of the model location. The behavior of the pattern during each run was recorded continuously with a videotape recorder and specific scenes were printed out with a video printer.

Liquid Crystal Visualization Technique

A liquid crystal method has some advantages for flow visualization over other techniques such as oil-flow method. Liquid crystals used in this investigation were of the microencapsulated cholesteric type and responded to temperature. Several applications of shear-sensitive liquid crystals have recently been shown,[8,9] but there have been few examples visualized with temperature-sensitive liquid crystals in a high Reynolds number transonic wind tunnel of the blowdown type. The liquid crystals have the following advantages: 1) they are easy to brush on the model surface because they are soluble in water, 2) they respond reversely and quickly to temperature, and 3) because of the dry surface they do not noticeably disturb the surface flow.

Application of liquid crystals to flow visualization requires consideration of the model and selection of proper liquid crystals. The model surface should be painted flat black for color contrast, and the surface coated with liquid crystals should be polished as smoothly as possible. The proper temperature range between the lowest (red color) and the highest (blue color) temperature, where liquid crystals scatter visible light, should be determined. For conditions in the NAL wind tunnel, a temperature range of about 2.5°C was judged to be suitable for visualizing aerodynamic phenomena. The liquid crystal visualization data were recorded with the video camera in the same way as the oil-flow visualization. Although delicate adjustment of the lighting and the viewing angle is additionally necessary, it is believed that this liquid crystal technique is suitable for visualizing subtle flow behavior such as a laminar separation bubble, which is otherwise difficult to detect.

Results and Discussions

Oil-Flow Visualization

A series of oil-flow visualization tests using three different chord models was conducted mainly at a Reynolds number

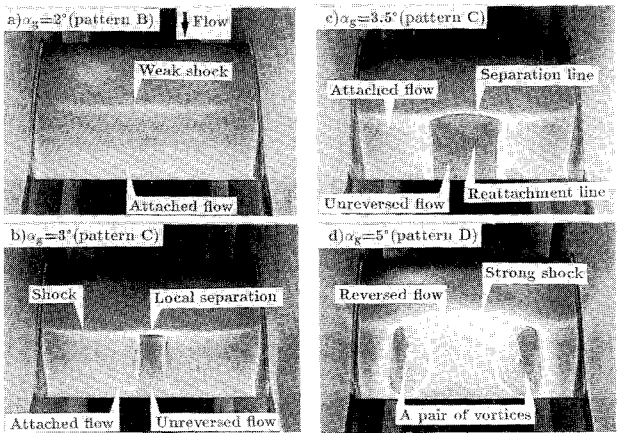

Fig. 2 Oil-flow photographs on the upper surface with varying the angle of attack for a model with an aspect ratio of 1.5; M_u = 0.75, Re = 21 × 10⁶.

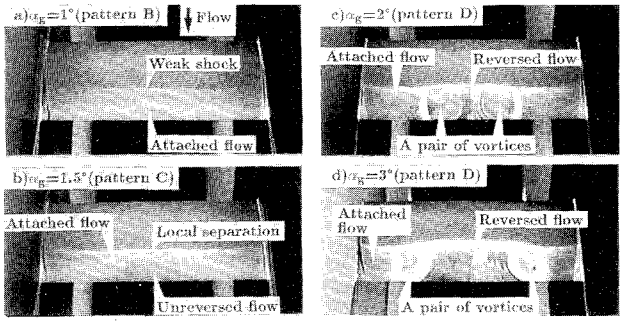

Fig. 3 Oil-flow photographs on the upper surface with varying the angle of attack for a model with an aspect ratio of 2.5; M_u = 0.78, Re = 21 × 10⁶.

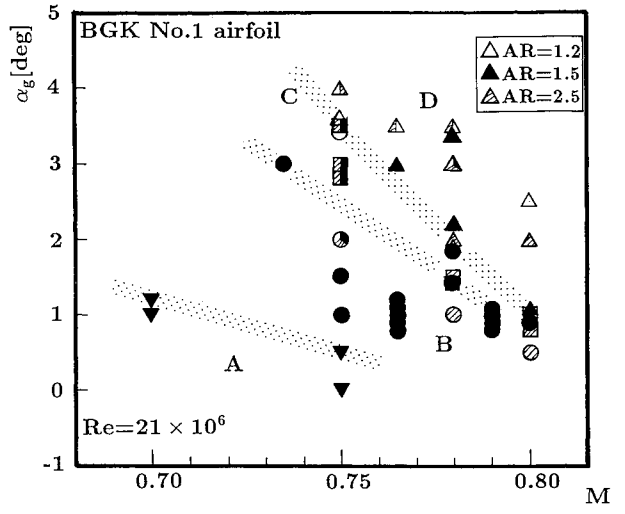

Fig. 4 Classification of oil-flow patterns in the transonic regime for three different chord models: A—inverted triangles, B—circles, C—squares, D—triangles.

(based on the airfoil chord) of 21 × 10⁶ in the transonic regime. The oil-flow pictures at various angles of attack on the upper surfaces of the models with aspect ratios of 1.5 and 2.5 are shown in Figs. 2 and 3, respectively. Classification of oil-flow patterns on another airfoil has been presented in Ref. 5. With respect to the BGK No. 1 airfoil, similar results were obtained. The flow patterns fall into the following four categories, as shown in Fig. 4.

A) Attached flow with no shock wave: In this case the flow attaches everywhere except in regions close to the sidewalls. The regions of the corner separation are, however, very narrow so that the main flow in the central region can be regarded as nearly two-dimensional.

B) Attached flow with a shock wave (Figs. 2a and 3a): In this case there exists a shock wave, and the oil accumulation is observed at the foot of the shock. Although the corner separation regions become wider and the shock moves slightly forward near the sidewalls, the main flow remains attached and two dimensional.

C) Separated but not reversed flow behind the shock (Figs. 2b, 2c, and 3b): Although a discontinuous oil accumulation line is observed at the foot of the shock, the flow behind the shock is still going downstream. This result reveals that the flow separates locally and reattaches. The flow near the sidewalls, on the other hand, remains attached. This is attributed to the displacement effects of the sidewall boundary layer.[5] The attached flow region is sensitive to freestream Mach number, angle of attack, Reynolds number, and the magnitude of the sidewall interference. In this article the sidewall effects mainly on pattern C are therefore discussed in detail.

D) Flow with trailing-edge separation (Figs. 2d, 3c, and 3d): In this case a pair of large vortices appears symmetrically behind the shock. The flow at the midspan is reversed and, thus, the shock moves forward. There is no longer a two-dimensional flow region, even for the higher aspect ratio model.

As shown in Fig. 4, the flow pattern changes from B into C at a moderate angle of attack. The local separation region of pattern C becomes wider as the angle of attack is increased. This result does not mean, however, that the two-dimensional region spreads in the spanwise direction. The reattachment line behind the local separation becomes three dimensional with the increase of angle of attack as indicated in Fig. 2c. When the flow separates on a large scale, the attached flow regions affected by the sidewalls are further reduced. The sidewall effects must therefore be evaluated at the point where the flow pattern begins to change from B to C. Figure 5 shows the effect of varying the Mach number on the spanwise length d_S of the attached region near the sidewall for the models with aspect ratios of 1.5 and 2.5. Irrespective of aspect ratio, regions within about 75% of the chord length from the sidewalls in the spanwise direction are affected by the sidewalls below the design Mach number (M_u = 0.772). The regions spread over one chord length with the increase of Mach number. It is noted that an aspect ratio of more than

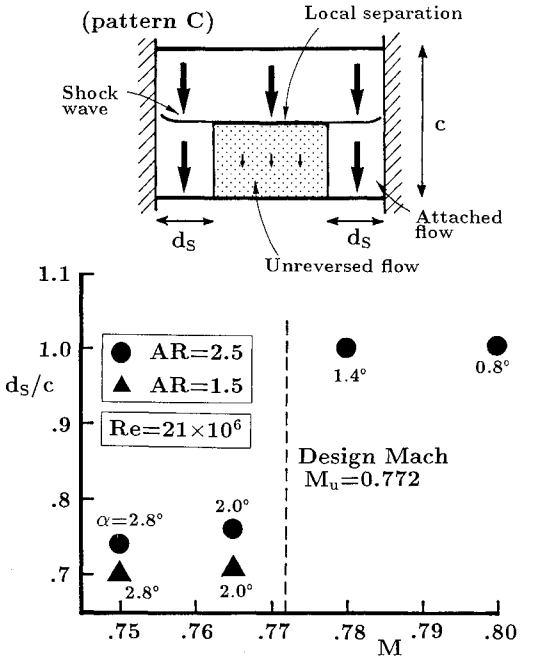

Fig. 5 Effect of varying the Mach number on the width of the attached region near the sidewall for models with aspect ratios of 1.5 and 2.5.

2 is necessary for maintaining the "two-dimensional" (not affected by the sidewall) region to some extent. Even if the tests are performed only below the design Mach number, an aspect ratio of no less than 1.5 is desirable.

Figure 6 shows oil-flow photographs for the three different chord models at a constant angle of attack that is corrected for the top and bottom wall effects.[10] Figure 6a represents the pattern of the ordinary aspect ratio (AR = 1.2) model in the NAL wind tunnel. Separated flow cannot be observed in the central region. With the higher aspect ratio models, however, the locally separated flow of pattern C can be recognized to some extent. This suggests that the sidewall boundary-layer effects extend over the whole surface of the low aspect ratio model and influence characteristics of the separation behind the shock. Proper choice of the airfoil aspect ratio is therefore necessary for reliable two-dimensional tests.

Liquid Crystal Visualization

A series of liquid crystal visualization tests was conducted at relatively low Reynolds numbers in order to examine the behavior of transition phenomena affected by the sidewalls. In these tests, the liquid crystals show the temperature variations on the model surface through changes in color (blue, green, and red). The temperatures of turbulent regions are lower than those of laminar regions. The visualized transition patterns on the upper surface of the BGK No. 1 airfoil at transonic speeds fall into three categories.

A) "Natural" transition: This pattern is observed at a negative angle of attack where a favorable pressure gradient extends over a wide region of the upper surface. The boundary layer becomes transitional, not separating from the surface, in the same process as on a flat plate at zero incidence.

B) Transition by a strong shock wave (Fig. 7): This pattern is observed where there exists a strong shock at a relatively forward position of the airfoil chord. An abrupt fall in temperature at the foot of the shock and a quick recovery of the temperature just behind the shock are observed. This suggests

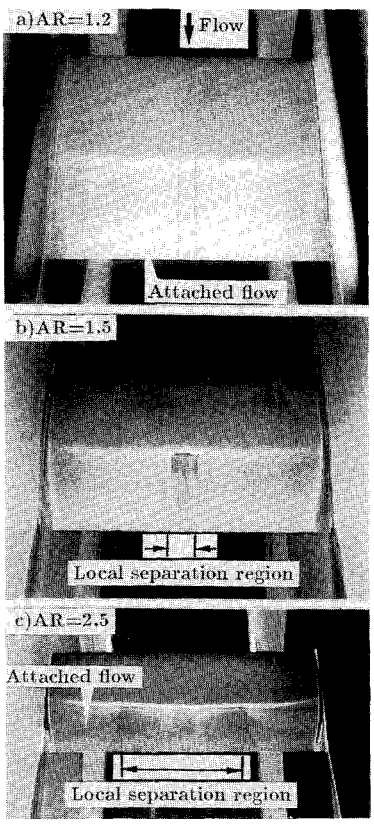

Fig. 6 Effect of varying the aspect ratio on oil-flow pattern at a corrected angle of attack for the top and bottom wall effects of 2.4 deg; M_u = 0.75, Re = 21 × 10^6.

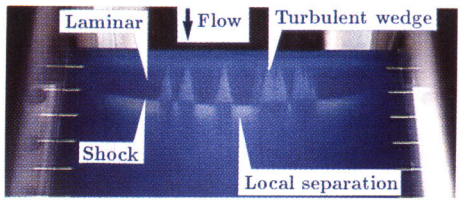

Fig. 7 Liquid crystal visualization for a transition phenomenon; M_u = 0.7, Re = 5.5 × 10^6, α_g = 3 deg, AR = 1.2.

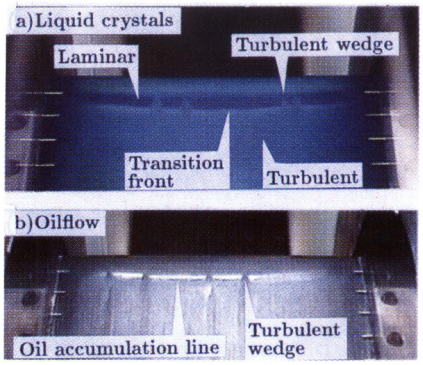

Fig. 8 Liquid crystal visualization for a transition phenomenon and the corresponding oil-flow picture; M_u = 0.78, Re = 5.5 × 10^6, α_g = 0 deg, AR = 1.2.

that the laminar boundary layer separates just ahead of the shock and reattaches to the surface in a turbulent state. In a turbulent wedge, on the other hand, the boundary layer approaching the shock is turbulent and does not separate from the surface, judging from the fact that only a temperature rise is observed at the foot of the shock.

C) Transition by a laminar separation bubble (Fig. 8a): This is observed where the strong shock is located at the backward position and there exists no steep adverse pressure gradient at the first half of the airfoil chord. As shown in Fig. 8a, a line with a few wedges is observed at about 16% of the chord. The corresponding oil-flow photograph (Fig. 8b) reveals the existence of the separation line at a location of about 4% chord length ahead of the indication of the liquid crystals. In contrast to pattern B, temperature rises behind the line and in a turbulent wedge cannot be recognized. These facts suggest the formation of a laminar separation bubble terminated by turbulent reattachment with no shock or a very weak shock. The line indicated by the liquid crystals corresponds to the reattachment line and is clearly visible as a straight line.

To investigate the sidewall effects on the transition behavior, the above-mentioned three patterns were investigated at various angles of attack. The results are shown in Fig. 9. The "natural" transition is not affected by the sidewall in particular as indicated in Fig. 9a. With respect to the transition by a strong shock wave (Fig. 9b), the transition front moves backward according to the shock position with the increase of angle of attack. Although the front is located forward near the sidewalls with the movement of the shock, a nearly two-dimensional region somewhat remains. With the transition by a laminar separation bubble (Fig. 9c), the sidewall boundary-layer effects become noticeable. The transition front can barely keep the two dimensionality only at α = 0 deg. As the angle of attack increases, however, the front at the midspan moves backward. For $\alpha \geq 1$ deg, oblique lines emanating from the leading edge near the sidewalls can be recognized. The picture for α = 3 deg is shown in Fig. 10. The location of the steep adverse pressure gradient tends to move backward, and the laminar region can extend over a wide region as the angle of attack increases. In supersonic flow regions, however, sidewall disturbances propagate in the form of waves from near the leading edge of the corners.[5] As a result, the laminar separation occurs along the disturbance waves and the tran-

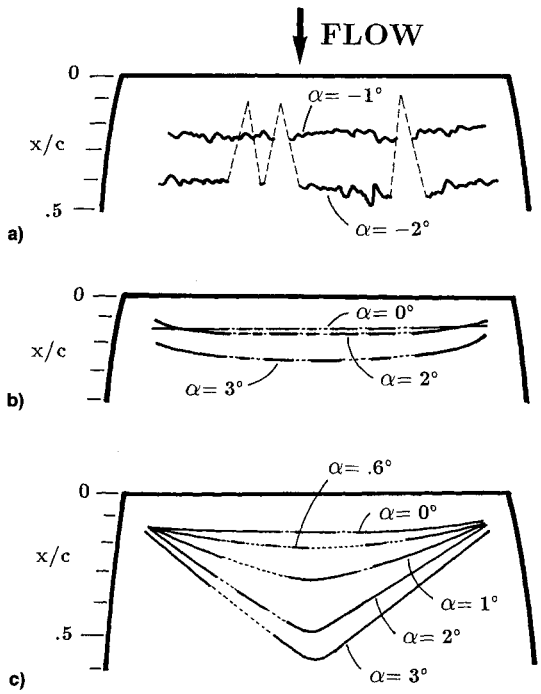

Fig. 9 Effect of varying the angle of attack on the transition phenomena: a) natural transition (M_u = 0.78, Re = 5.5 × 10⁶), b) transition by a strong shock wave (M_u = 0.7, Re = 5.5 × 10⁶), and c) transition by a laminar separation bubble (M_u = 0.78, Re = 5.5 × 10⁶).

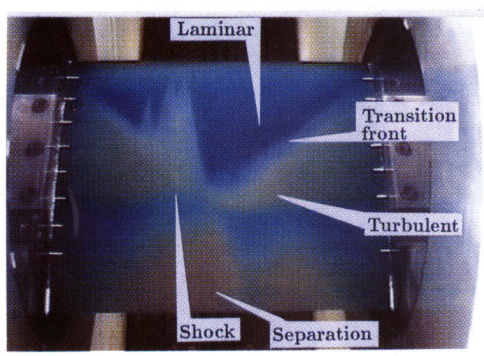

Fig. 10 Liquid crystal visualization for the transition phenomenon affected strongly by the sidewalls; M_u = 0.78, Re = 5.5 × 10⁶, α_g = 3 deg, AR = 1.2.

sition fronts appear as oblique lines. In these cases, a two-dimensional region can no longer be recognized anywhere. Figure 10 shows also that the strong shock at about 60% of the chord is distorted by whether the approaching boundary layer is laminar or turbulent. The transition behavior strongly influences the two dimensionality of the shock and the separation behind it.

The three dimensionality of the transition leads to an undesirable result on drag measurement for low aspect ratio airfoil testing as shown in Fig. 11. The drag coefficients are deduced from the data measured using a wake rake positioned at a distance of about 500 mm behind the airfoil trailing edge. The data are measured with two total pressure tubes of the rake at spanwise positions of 30 and 80 mm from the central section [$y/(b/2)$ = 0.2 and 0.533, respectively]. The solid symbols denote drag coefficients at the inner section, and the open symbols denote those at the outer section. For a high Reynolds number where the transition occurs two dimensionally very close to the leading edge (Re > 7 × 10⁶), the inner section drag tends to be a little larger than the outer one. For Re < 7 × 10⁶ and high angles of attack, however, the outer section drag becomes larger than the inner one as the angle of attack increases. This inversion of the section

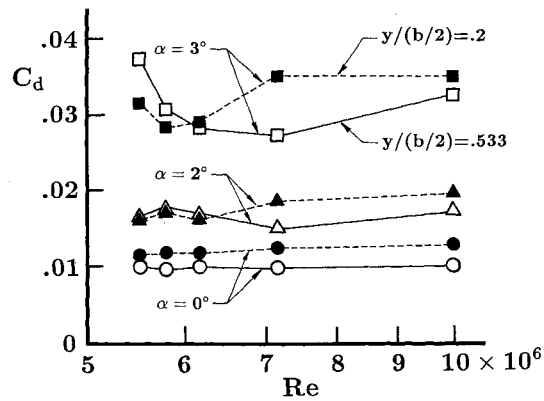

Fig. 11 Sidewall effects on spanwise section drag coefficients deduced from the wake measurements; M_u = 0.78, AR = 1.2.

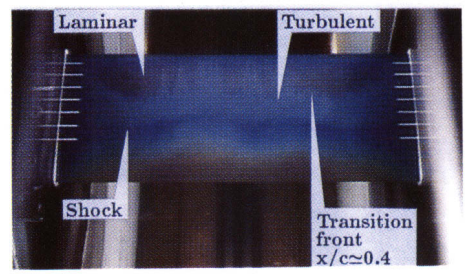

Fig. 12 Liquid crystal visualization for a model with a high aspect ratio of 2.5; M_u = 0.78, Re = 5.5 × 10⁶, α_g = 2.7 deg.

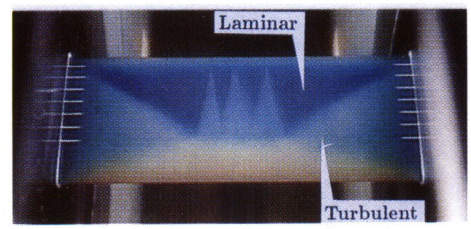

Fig. 13 Liquid crystal visualization for a model with a high aspect ratio of 2.5; M_u = 0.78, Re = 3 × 10⁶, α_g = 0.8 deg.

drag coefficients appears just when the three dimensionality of the transition becomes noticeable. The increase of the outer section drag compared to the inner one is attributed to the expanse of the turbulent region near the sidewall. The sidewall effects that extend to the central section, affecting the separation phenomenon behind the shock, result in the slight increase of the inner section drag at α = 3 deg and Re = 5.5 × 10⁶.

Figure 12 shows the visualization result for the higher aspect ratio model at the same corrected angle of attack as that for the model shown in Fig. 10. The transition front appears as oblique lines just within about 50% of the chord length from the sidewalls, while the transition occurs two dimensionally at about 40% of the chord in the main flow region. For a lower Reynolds number of 3 × 10⁶ (Fig. 13), however, the sidewall disturbances dominate the transition behavior as well as in Fig. 10. The oblique transition front reaches the central region even for the aspect ratio of 2.5. This aspect ratio is by no means sufficient for attainment of the two-dimensional transition behavior. The liquid crystal visualization data suggest the necessity of a considerably high aspect ratio model, especially for low Reynolds number testing.

Effects of Sidewall Boundary-Layer Suction

In order to minimize the sidewall effects, most two-dimensional wind tunnels are equipped with sidewall boundary-layer removal systems.[11,12] In the NAL wind tunnel, however, the system has not been activated for ordinary tests because recent calibration tests showed that the sidewall boundary-layer suc-

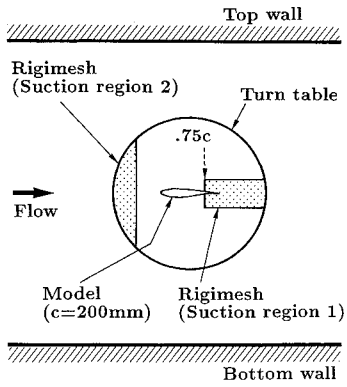

Fig. 14 Regions of the sidewall boundary-layer suction: 1—region behind the 75% airfoil chord location and 2—region ahead of the model.

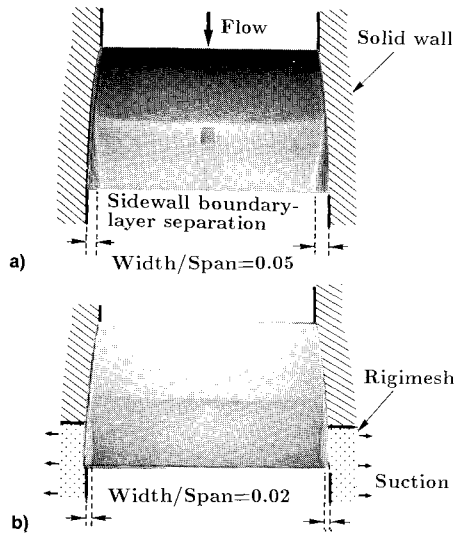

Fig. 15 Effect of downstream suction (only region 1 illustrated in Fig. 14) on model surface flow; M_u = 0.75, Re = 21 × 10^6, α_g = 2.8 deg: a) without suction and b) with suction.

tion in the vicinity of the model (in the whole region of the turn table illustrated in Fig. 14) induced axial Mach number nonuniformity in the flow direction with a maximum deviation of 0.015.[13] The local suction just at the regions where there exist strong viscous effects of the sidewall boundary layer has therefore been examined. The regions of the suction are illustrated in Fig. 14. Two kinds of suction were tried in the present investigation: 1) the region behind the location of 75% airfoil chord, with the aim of reducing the separation region of the sidewall boundary layer, and 2) the region ahead of the model, with the aim of thinning the sidewall boundary-layer thickness at the model location.

The effects of the downstream suction on the airfoil surface flow are shown in Fig. 15. Compared with the pattern without the suction, the downstream suction significantly reduces the separation region near the sidewall. It cannot, however, change the flow in the central region and, moreover, it is effective at a relatively low angle of attack only. As indicated in Fig. 16, on the other hand, the upstream suction drastically spreads the central local separation region, which is regarded as being little affected by the sidewalls.

Although the suction leads to significant effects on the surface flow, there is room for doubt that it is effective in measuring pressure at the central section. Actually, no noticeable change in pressure distribution caused by the suction could be recognized from the NAL wind-tunnel tests. The suction in this investigation is by no means the best, and detailed examination on the suction flow rate is also required. The

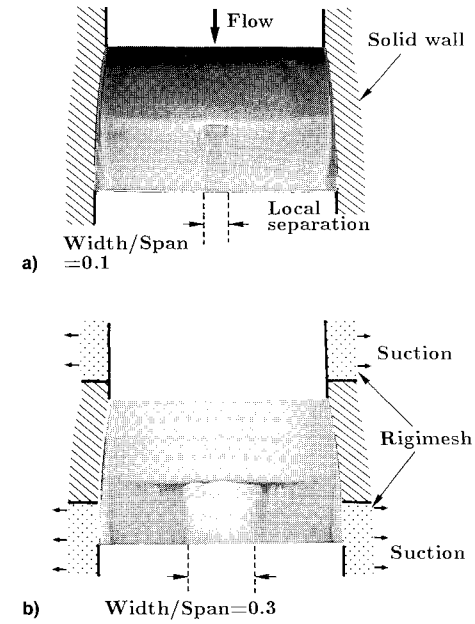

Fig. 16 Effect of upstream and downstream suction (both regions 1 and 2 illustrated in Fig. 14) on model surface flow; M_u = 0.75, Re = 21 × 10^6, α_g = 3 deg: a) without suction and b) with suction.

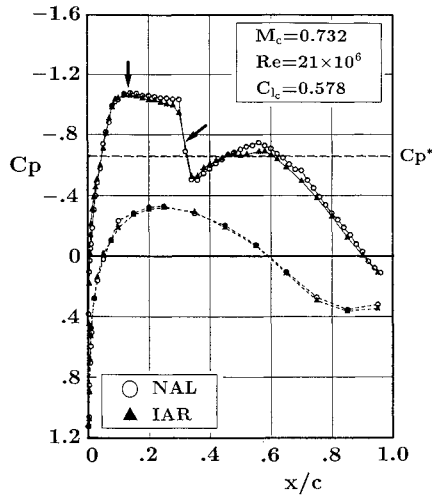

Fig. 17 Comparison of pressure distributions with the same lift coefficient at a corrected Mach number for the four-wall effects of 0.732.

sidewall effects are, however, expected to remain even if the proper suction is performed.

Correction for Sidewall Interference

To assess the applicability of sidewall interference correction, the Murthy method was applied to both the NAL and IAR data. The application of the method to NACA 0012 airfoil data has already led to significant results in the NAL wind tunnel.[14] Figure 17 shows a comparison of pressure distributions corrected for the four-wall effects. Both data are corrected for the top and bottom wall effects and, furthermore, for the sidewall effects by the Murthy method. To apply the Murthy method, values of displacement thickness and shape factor of the sidewall boundary layer are necessary. The values measured in the empty tunnel calibration tests are used for correction of the NAL data. With respect to the IAR data, the maximum value taken from Ref. 15 for the sidewall boundary-layer displacement thickness and the typical value of 1.5 for the shape factor in transonic turbulent boundary layer are used. Although the IAR data contain the sidewall boundary-layer suction, its effects are ignored in this investigation. Figure 17 reveals that applying the correction elim-

inates the slight difference in shock position and suction peak level ahead of the shock, and that it improves agreement drastically in comparison with Fig. 1. The result suggests that it is very promising to apply the Murthy correction to both sets of tunnel data. Although the application removes the discrepancies in data obtained from different tunnels, there still remain some difficult problems, such as the validity of the corrected Mach number. Furthermore, how the effect of the suction should be dealt with in the procedure of the correction is one of the most important problems. In order to conduct reliable two-dimensional tests, comprehensive research on the combination of the best experimental technique and the most suitable wall correction will be required.

Concluding Remarks

Flow visualization tests using oil-flow and liquid crystal methods were conducted to assess the effects of the sidewall boundary layer on the BGK No. 1 airfoil. The results can be summarized as follows:

1) Oil-flow visualization results showed four flow patterns and revealed that the sidewall effects strongly influenced the spanwise width of the local separation in the central region for a relatively high angle of attack. Close inspection of the local separation using three different chord models indicated that a model for airfoil testing should have an aspect ratio of at least 1.5 even for relatively low Mach number tests. Especially for tests at a high Mach number, an aspect ratio of more than 2.0 is necessary.

2) Liquid crystal visualization revealed that transition by a laminar separation bubble was susceptible to sidewall effects, and that the three dimensionality of the transition behavior strongly affected drag measurements in the wake. These visualization results also suggested the necessity of a high aspect ratio for an airfoil test model.

3) Sidewall boundary-layer suction was effective in reducing the corner separation region near the sidewall and spreading the central local separation region that was believed to be little affected by the sidewalls.

4) Applying a sidewall correction removed discrepancies between data of the two wind tunnels in shock position and pressure level ahead of the shock, and led to satisfactory agreement between the two sets of data.

One of the most important tasks in future development of aircraft is to conduct more reliable two-dimensional airfoil tests with higher accuracy, clarifying uncertainties that still remain in wind-tunnel testing. For this objective, comprehensive research including investigations on model aspect ratio, sidewall boundary-layer suction technique, and wall interference correction will be required.

Acknowledgments

This research was carried out as part of a comparative study between the Institute for Aerospace Research of Canada and the National Aerospace Laboratory of Japan. The authors wish to acknowledge Y. Y. Chan and his staff of the IAR High Speed Aerodynamics Laboratory for helpful discussions on part of the experimental results.

References

[1]Plosenski, M. J., Jones, D. J., Mokry, M., and Ohman, L. H., "Supplementary Investigation of the BGK No. 1 Airfoil; Wall Interference Study, ADDENDUM; Tabulated Data Corrected for Wall Interference," National Research Council, LTR-HA-5×5/0127, Ottawa, Canada, Aug. 1981.

[2]Barnwell, R. W., "A Similarity Rule for Compressibility and Sidewall-Boundary-Layer Effects in Two-Dimensional Wind Tunnels," AIAA Paper 79-0108, Jan. 1979.

[3]Sewall, W. G., "Effects of Sidewall Boundary Layers in Two-Dimensional Subsonic and Transonic Wind Tunnels," *AIAA Journal*, Vol. 20, No. 9, 1982, pp. 1253–1256.

[4]Murthy, A. V., "Effects of Aspect Ratio and Sidewall Boundary-Layer in Airfoil Testing," *Journal of Aircraft*, Vol. 25, No. 3, 1988, pp. 244–249.

[5]Su, Y., "Mechanism of Sidewall Effect Studied with Oil Flow Visualization," *AIAA Journal*, Vol. 27, No. 12, 1989, pp. 1828–1830.

[6]The Staff of the Second Aerodynamics Division, "Construction and Performance of NAL Two-Dimensional Transonic Wind Tunnel," National Aerospace Lab. TR-647T, Tokyo, Japan, Feb. 1982.

[7]Kacprzynski, J. J., Ohman, L. H., Garabedian, P. R., and Korn, D. G., "Analysis of the Flow Past a Shockless Lifting Airfoil in Design and Off-Design Conditions," National Research Council, LR-554, Ottawa, Canada, Nov. 1971.

[8]Reda, D. C., "Observations of Dynamic Stall Phenomena Using Liquid Crystal Coatings," *AIAA Journal*, Vol. 29, No. 2, 1991, pp. 308–310.

[9]Smith, S. C., "Use of Shear-Sensitive Liquid Crystals for Surface Flow Visualization," *Journal of Aircraft*, Vol. 29, No. 2, 1992, pp. 289–293.

[10]Sawada, H., Sakakibara, S., Sato, M., and Kanda, H., "Wall Interference Estimation of the NAL's Two-Dimensional Wind Tunnel" (in Japanese), National Aerospace Lab. TR-829, Tokyo, Japan, Aug. 1984.

[11]Galway, R. D., "The IAR High Reynolds Number Two-Dimensional Test Facility—A Description of Equipment and Procedures Common to Most 2-D Airfoil Tests," National Research Council, IAR-AN-66, Ottawa, Canada, June 1990.

[12]Murthy, A. V., Johnson, C. B., Ray, E. J., and Stanewsky, E., "Investigation of Sidewall Boundary Layer Removal Effects on Two Different Chord Airfoil Models in the Langley 0.3-Meter Transonic Cryogenic Tunnel," AIAA Paper 84-0598, March 1984.

[13]Kawamoto, I., Miwa, H., Baba, S., Sato, M., Kanda, H., and Sudani, N., "Recent Airfoil Tests in NAL 2D High Reynolds Number Wind Tunnel," *Proceedings of the 28th Aircraft Symposium*, Japan Society for Aeronautical and Space Sciences, Tokyo, Japan, 1990, pp. 346–349.

[14]Sudani, N., Kanda, H., Sato, M., Miwa, H., Matsuno, K., and Takanashi, S., "Evaluation of NACA0012 Airfoil Test Results in the NAL Two-Dimensional Transonic Wind Tunnel," National Aerospace Lab. TR-1109T, Tokyo, Japan, May 1991.

[15]Ohman, L. H., and Brown, D., "The NAE High Reynolds Number 15in. × 60in. Two-Dimensional Test Facility, Part II. Results of Initial Calibration," National Research Council, LTR-HA-4, Ottawa, Canada, Sept. 1970.